DALTON

# *trans* Effect and *trans* influence of triphenyl-stibine and -phosphine in platinum(II) complexes. A comparative mechanistic and structural study ‡

**Ola F. Wendt and Lars I. Elding *,†**

*Inorganic Chemistry 1, Chemical Center, Lund University, PO Box 124, S-221 00 Lund, Sweden*

The kinetics and mechanism of the reactions between *trans*-$[PtI_3(PPh_3)]^-$ and *trans*-$[PtI_3(SbPh_3)]^-$ with pyridine, 2- and 4-methylpyridine in acetonitrile solvent have been studied by stopped-flow spectrophotometry. The crystal and molecular structures of the tetrabutylammonium salts of the two anions have been determined. Substitution of iodide *trans* to stibine is reversible and takes place *via* parallel direct and solvolytic pathways; substitution in the phosphine complex occurs with negligible back reaction. The kinetic data indicate that triphenyl-stibine and -phosphine should be placed in a series of decreasing *trans* effect, $C_2H_4 > SbPh_3 > CO > P(OMe)_3 > PPh_3 > AsEt_3$, *i.e.* $SbPh_3$ has a much larger *trans* effect than that of $PPh_3$; stibine complexes in the present study react *ca.* 16 times faster than their phosphine analogues. The activation parameters are typical of associatively activated processes, and in the case of the stibine complex they indicate that very little bond breaking has occurred in the transition state. In the ground states there is a clear-cut difference in the Pt–I distances *trans* to the pnictogen, 2.637(2) Å in the stibine complex and 2.662(3) Å in the phosphine complex, indicating that $SbPh_3$ has a smaller ground-state *trans* influence and hence is a weaker σ donor than $PPh_3$. Since the kinetic *trans* effect is a combination of ground-state labilisation and transition-state stabilisation, it is concluded that the large *trans* effect of stibine is due to a better π acceptance. Based on a comparison of Sb–C distances and C–Sb–C angles in free and co-ordinated stibine, this is proposed to be due to a higher d character of the π* orbitals on stibine as compared to phosphine, leading to a better overlap between antimony π* and platinum 5d π orbitals.

In contrast to the many phosphine and arsine complexes of platinum(II) that have been prepared and investigated, kinetic data on platinum(II) stibine complexes are scarce.[1,2] To our knowledge only one qualitative investigation dealing with the *trans* effect of stibine has appeared. It was concluded that the $SbPh_3$ ligand has a slightly higher *trans* effect than that of triphenylphosphine.[3] In addition, very little structural work on platinum(II) stibine complexes has been published,[4] so the assessment of the ground-state *trans* influence of stibine ligands has been based mainly on spectroscopic data.[4–6] In the context of our current mechanistic and structural studies of platinum(II) complexes with Group 14 and 15 donor ligands[7–9] we have undertaken a kinetic and structural study of some triphenylstibine complexes in order to evaluate quantitatively the *trans* effect and ground-state *trans* influence of this ligand.

The reactions of heterocyclic amines and other nucleophiles with complexes of the type $[PtCl_3L]^-$ have been investigated for a large number of neutral ligands L and their *trans* effects have been determined.[10–14] Previous work has also aimed at subdividing the *trans* effect into its σ and π components by means of an analysis of the nucleophilic discrimination. In the present case it was therefore natural to choose a similar system for investigation. The kinetics and mechanism for the reaction of $[PtI_3(EPh_3)]^-$ (E = P or Sb) with pyridine and substituted pyridines have been studied in acetonitrile solution, together with the crystal structures of $[NBu_4][PtI_3(EPh_3)]$ (E = P or Sb).

## Experimental

### General procedures and materials

The complexes $[NBu_4]_2[Pt_2Cl_6]$, $[NBu_4]_2[Pt_2I_6]$ and $[Pt_2Cl_4(PPh_3)_2]$ were prepared according to the literature.[15–17] Pyridine (Kebo, purum), 2- (Acros 98%) and 4-methylpyridine (Merck zS) were refluxed over KOH pellets and distilled prior to use. Triphenylphosphine (Merck) was recrystallised from EtOH. Triphenylstibine (Acros 97%), sodium iodide (Merck pa), tetrabutylammonium iodide (Merck zS), $PtCl_2$ (Degussa), $K_2[PtCl_4]$ (Degussa) and all solvents (LabScan AR) were used without further purification. Elemental analysis was performed by Mikro Kemi AB, Uppsala, Sweden. The IR spectra were recorded as polyethylene pellets on a Bio-Rad FTS 6000 FT-IR spectrometer, Raman spectra on a Bio-Rad FT-Raman spectrometer and NMR spectra on a Varian Unity 300 spectrometer; WALTZ-16 $^1H$ decoupling was used in the non-$^1H$ nuclei experiments. Chemical shifts are given in ppm downfield from $SiMe_4$ ($^1H$), $H_3PO_4$ ($^{31}P$) and $K_2[PtCl_6]$ ($^{195}Pt$). Residual solvent peaks ($^1H$), $H_3PO_4$ ($^{31}P$) and $K_2[PtCl_4]$ ($^{195}Pt$, δ −1639) were used as internal and external standards, respectively. Spectroscopic data for the complexes are given in Tables 1 and 2.

### Preparations

**$[NBu_4][PtI_3(SbPh_3)]$ 1.** A sample of $[NBu_4]_2[Pt_2I_6]$ (0.507 g, 0.310 mmol) was dissolved in $CH_2Cl_2$ (15 $cm^3$). A solution of $SbPh_3$ (0.215 g, 0.610 mmol) in $CH_2Cl_2$ (15 $cm^3$) was added dropwise and the resulting solution was stirred at room temperature for 1 h. The solvent was evaporated and the crude product recrystallised from $CH_2Cl_2$–diethyl ether, yielding 0.620 g (85%) (Found: C, 35.0; H, 4.4; N, 1.2. Calc. for $C_{34}H_{51}I_3NPtSb$: C, 34.9; H, 4.4; N, 1.2%). NMR ($CD_2Cl_2$): $^1H$ (299.79 MHz), δ 1.01 (t, $J$ = 7.4 Hz, 12 H), 1.38–1.51 (m, 8 H), 1.58–1.74 (m, 8 H), 3.15–3.28 (m, 8 H), 7.30–7.49 (m, 9 H) and 7.65–7.76 (m, 6 H); $^{195}Pt$ (64.08 MHz), δ −5717 (s).

**$[NBu_4][PtI_3(PPh_3)]$ 2.** A sample of $[Pt_2Cl_4(PPh_3)_2]$ (0.640 g, 0.606 mmol) was refluxed with NaI (0.424 g, 2.83 mmol) for 2 h in acetone (≈15 $cm^3$). The solvent was evaporated, $CH_2Cl_2$ was added and the solution was filtered. An amount of $NBu_4I$ (0.972 g, 2.63 mmol) was added and the solution was stirred at

† E-Mail: LarsI.Elding@inorg.lu.se

‡ *Supplementary data available* (No. SUP 57316, 5 pp.): pseudo-first-order rate constants and equilibrium absorbances. See Instructions for Authors, *J. Chem. Soc.*, *Dalton Trans.*, 1997, Issue 1.

**Table 1** Spectroscopic data for $[PtI_3(PPh_3)]^-$ **2**, *trans*-$[PtI_2(PPh_3)(py)]$ **4**, *trans*-$[PtI_2(PPh_3)(2\text{-mpy})]$ **6**, *trans*-$[PtI_2(PPh_3)(4\text{-mpy})]$ **7** and $[Pt_2I_4(PPh_3)_2]$ **8**

| | | **2**[a] | **4** | **6** | **7** | **8** |
|---|---|---|---|---|---|---|
| $^{31}$P NMR | δ | 13.7 | 0.60 | 1.5[b] | −1.20 | 14.7 |
| | $^1J_{PtP}$/Hz | 3619 | 3365 | 3417 | 3355 | 3686 |
| IR/cm$^{-1}$ | ν($PtI_2$), $A_1$ | 154w | *c* | | | |
| | ν($PtI_2$), $B_1$ | 196vs | 200s(?) | | | |
| | ν(PtI) | 187 (sh) | | | | |
| Raman/cm$^{-1}$ | ν($PtI_2$), $A_1$ | 156vs | 151vs | | | |
| | ν($PtI_2$), $B_1$ | *c* | 188w | | | |
| | ν(PtI) | 188w | | | | |

[a] The NMR spectrum was recorded in the presence of free iodide. [b] In addition the spectrum of the mixture of complex **2** and 2-mpy contains an unidentified peak at δ 9.8 ($^1J_{PtP}$ = 3631 Hz). [c] Zero intensity.

room temperature overnight. The solvent was evaporated and the crude product recrystallised from $CH_2Cl_2$–diethyl ether twice, yielding 0.692 g (53%) (Found: C, 37.6; H, 4.6; N, 1.3. Calc. for $C_{34}H_{51}I_3NPPt$: C, 37.8; H, 4.8; N, 1.3%). NMR ($CD_2Cl_2$): $^1$H (299.79 MHz), δ 1.00 (t, $J$ = 7.4 Hz, 12 H), 1.36–1.51 (m, 8 H), 1.56–1.71 (m, 8 H), 3.15–3.26 (m, 8 H) and 7.28–7.82 (m, 15 H); $^{195}$Pt (64.08 MHz), δ −5639 (d, $^1J_{PtP}$ = 3617 Hz).

***trans*-[$PtI_2(SbPh_3)(py)$] 3.** A sample of compound **1** (0.090 g, 0.077 mmol) was dissolved in MeCN (15 cm$^3$). Pyridine (py, 0.050 cm$^3$) was added and the solution stirred for 1 h. The solution was evaporated to half of its original volume and kept in a freezer for 24 h. The orange crystals formed were collected on a filter. Yield: 0.049 g (72%) (Found: C, 31.6; H, 2.4; N, 1.5. Calc. for $C_{23}H_{20}I_2NPtSb$: C, 31.3; H, 2.3; N, 1.6%). $^1$H NMR ($CD_2Cl_2$, 299.79 MHz): δ 7.38–7.51 (m, 11 H), 7.66–7.74 (m, 6 H), 7.84 (tt, $J$ = 7.6, 1.5, *p*-H) and 9.07–9.13 (m, 2 H, $^3J_{PtH} \approx 36$ Hz, *o*-H).

***trans*-[$PtI_2(PPh_3)(py)$] 4.** Compound **4** was prepared similarly to **3** from **2** (0.063 g, 0.058 mmol), NaI (0.081 g, 0.54 mmol) and pyridine (0.050 cm$^3$). Yield: 0.038 g (84%) (Found: C, 34.6; H, 2.6; N, 2.0. Calc. for $C_{23}H_{20}I_2NPPt$: C, 35.0; H, 2.6; N, 1.8%). $^1$H NMR ($CD_2Cl_2$, 299.79 MHz): δ 7.38–7.52 (m, 11 H), 7.75–7.88 (m, 7 H) and 8.91–8.96 (m, 2 H).

### Crystallography

Single crystals of complexes **1** and **2** suitable for X-ray diffraction were obtained by allowing diethyl ether slowly to evaporate into dichloromethane solutions of the complexes. Intensity data were collected at room temperature on an Enraf-Nonius CAD-4 diffractometer with graphite-monochromated Mo-Kα radiation (λ = 0.710 69 Å) using the ω–2θ scan technique. Three standard reflections were measured at regular intervals and data corrected for decay. Unit-cell dimensions were obtained from 15 reflections. The heavy atoms were located with the Patterson method. Fourier-difference maps revealed the remaining atoms and the structures were refined by full-matrix least-squares calculations using the TEXSAN crystallographic software package.[18] The function minimised was $\Sigma w(|F_o| - |F_c|)^2$ with weights $w = 1/\sigma^2(F)$; $I$ and $\sigma(I)$ were corrected for Lorentz-polarisation and absorption effects (ψ scans). All non-hydrogen atoms were refined anisotropically. The hydrogen atoms in the phenyl rings were placed at calculated positions and included in the structure-factor calculations. The maximum residual electron densities were found 1.13 and 1.07 Å from the platinum atom in **1** and **2**, respectively. Crystal data and detailed experimental information are given in Table 3.

CCDC reference number 186/774.

### Kinetics

The stopped-flow experiments were performed on an Applied Photophysics Bio Sequential SX-17 MX, stopped-flow spectrofluorimeter. The substitution of iodide in complex **1** or **2** by various amines was studied in acetonitrile solvent by observing the decrease in absorbance at 361 or 385 nm, respectively. The complex solution [(1–3) × 10$^{-4}$ mol dm$^{-3}$] containing an excess of iodide [(4–50) × 10$^{-3}$ mol dm$^{-3}$] was mixed directly in the stopped-flow instrument with an equal volume of amine solution, resulting in at least a ten-fold excess of entering ligand [(7–80) × 10$^{-3}$ mol dm$^{-3}$], assuring pseudo-first-order conditions. The kinetic traces were fitted by single exponentials using the software provided by Applied Photophysics,[19] resulting in observed rate constants at different concentrations of leaving and incoming ligand. Rate constants are given as an average from at least five runs. Time-resolved spectra were also recorded on the Applied Photophysics instrument. Variable-temperature experiments were performed between 288 and 315 K. Complete data have been deposited (SUP 57316).

### UV/VIS equilibrium measurements

The UV/VIS spectra were recorded on a Milton Roy 3000 diode-array spectrophotometer. The equilibrium absorbance in the solvolysis of complex **1** according to reaction (1) given below was measured for different [I$^-$]. That for the reaction between **1** and pyridines according to reaction (3) below was derived from the amplitude of the kinetic traces at different [I$^-$] and [am]. In this case the absorbance is given as an average from at least five runs. Complete data have been deposited (SUP 57316).

## Results

### Synthesis

The triphenylphosphine complex **2** was prepared using a method earlier employed for the corresponding chloro complex.[13] The dinuclear iodo-bridged bis(phosphine) complex $[Pt_2I_4(PPh_3)_2]$ was cleaved with $NBu_4I$ to yield **2**. This method is not operable for the synthesis of stibine complexes, due to their thermal instability; all our attempts to prepare the analogous dinuclear iodo-bridged stibine complex yielded platinum black. Instead the $[Pt_2I_6]^{2-}$ ion was cleaved by use of a stoichiometric amount of $SbPh_3$, which gave **1** as the only product. One reason for using iodo- instead of chloro-complexes was that the aforementioned reaction works poorly starting from $[Pt_2Cl_6]^{2-}$.

### Vibrational spectra

The complexes were characterised by their IR and Raman spectra. The most diagnostic vibrations are the Pt–I stretching vibrations given in Tables 1 and 2. The symmetry of the complexes {whether $[PtI_3L]$ or *trans*-$[PtI_2L(L')]$} is $C_{2v}$ and hence four stretching vibrations were anticipated, all of which should be both IR and Raman active. For $[PtI_3L]$ three of those are mostly Pt–I in character, whereas for *trans*-$[PtI_2L(L')]$ there are two Pt–I vibrations.

Spectral assignment was first made for the phosphine complexes, since their spectra are assumed to contain the least amount of coupling. The strongest Raman band is normally the symmetric ν(Pt–$I_2$) and a very strong band a little above 150 cm$^{-1}$, present for all complexes, was assigned to this vibration.

**Table 2** Spectroscopic data for $[PtI_3(SbPh_3)]^-$ **1**, *trans*-$[PtI_2(SbPh_3)(py)]$ **3** and *trans*-$[PtI_2(2\text{-mpy})(SbPh_3)]$ **9**

| | | **1** | **3** | **9** |
|---|---|---|---|---|
| IR/cm$^{-1}$ | $\nu(PtI_2)$, $A_1$ | * | 153vw | * |
| | $\nu(PtI_2)$, $B_1$ | 197m | 183s | 188m |
| | $\nu(PtI)$ | 178s | | |
| Raman/cm$^{-1}$ | $\nu(PtI_2)$, $A_1$ | 154vs | 153vs | 152vs |
| | $\nu(PtI_2)$, $B_1$ | * | 183vw | * |
| | $\nu(PtI)$ | * | | |

* Zero intensity.

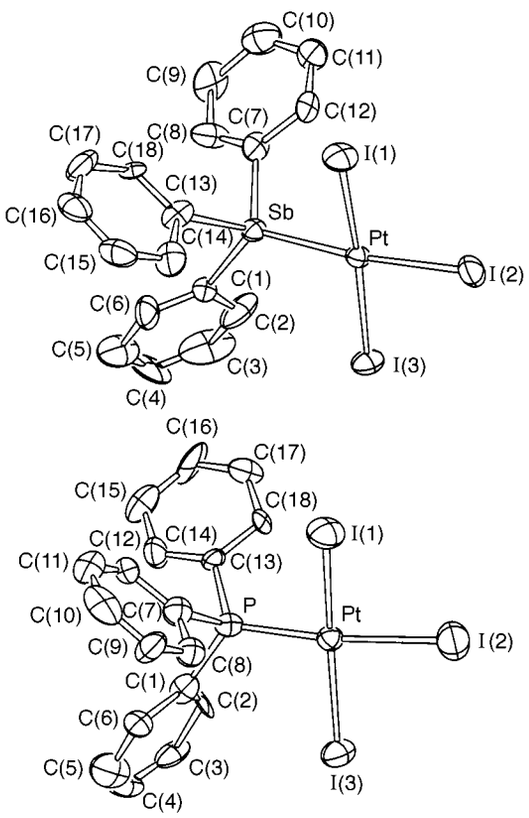


**Fig. 1** The ORTEP[21] drawings with atomic numbering of the structures of the anionic complexes $[PtI_3(SbPh_3)]^-$ **1** (top) and $[PtI_3(PPh_3)]^-$ **2** (bottom). The ellipsoids denote 40% probability. The tetrabutylammonium cations were omitted for clarity

This band is normally weak in the IR, whereas the asymmetric $\nu(Pt–I_2)$, which is weak or absent in the Raman spectrum, often provides the strongest vibration.[20] The strongest band in the IR spectrum was assigned accordingly. Based on this information all the bands in the spectra of the phosphine complexes could be assigned, except for one at 187 cm$^{-1}$ in the IR spectrum of **4**. The spectra of the stibine complexes were treated analogously.

### Crystal structures

The anionic complexes **1** and **2** are isostructural and their structures are given in Fig. 1. The co-ordination geometry around platinum is distorted square planar with angles ranging from 85.8 to 92.7° in **1** and from 87.1 to 95.5° in **2**. The largest deviation from a least-squares plane through $PtI_3E$ is 0.13 Å in **1** [I(1) and I(2)] and 0.24 Å in **2** (P). Both crystals are weak scatterers with 42% observed reflections for **1** [$I/\sigma(I) > 2.5$] and 32% [$I/\sigma(I) > 2.0$] for **2**. Selected bond distances and angles are given in Table 4.

### Solvolysis

The UV/VIS spectrum of complex **1** dissolved in MeCN changes when free iodide is added and peaks at 361 and 407 nm grow in. These spectral changes are best explained by a solvolytic equilibrium (1). This is fast ($t_{\frac{1}{2}} < ca.$ 50 ms for the

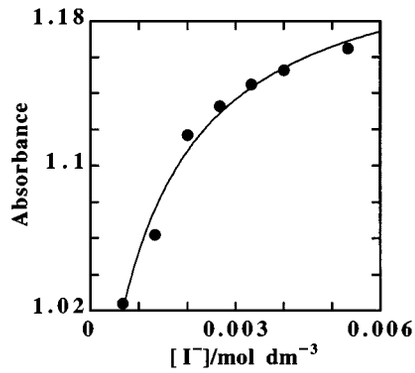


**Fig. 2** Equilibrium absorbance for the solvolytic reaction (1) as a function of iodide concentration. $T = 25$ °C, $[Pt] = 0.52 \times 10^{-3}$ mol dm$^{-3}$

$$[PtI_3(SbPh_3)]^- + MeCN \underset{k_{31}}{\overset{k_{13}}{\rightleftharpoons}} [PtI_2(SbPh_3)(MeCN)] + I^- \quad (1)$$

**1** **5**

conditions used) and its equilibrium constant, $K_s$, was determined by measuring the absorbance at 361 nm at different iodide concentrations. Assuming a constant $[I^-]$ during the reaction, equation (2), where $A_\infty$ (the absorbance at infinite

$$A = \frac{A_\infty[I^-] + \varepsilon_M K_s[Pt]}{K_s[I^-]} \quad (2)$$

$[I^-]$), $\varepsilon_M$ (the absorption coefficient of **5** at the pathlength used) and $K_s$ are the adjustable parameters, was fitted to the data. The fit (Fig. 2) gave $K_s = (1.0 \pm 0.6) \times 10^{-3}$ mol dm$^{-3}$.

Complex **2** is much less sensitive to solvolysis. Dissolving **2** in either a co-ordinating or a non-co-ordinating solvent gives two peaks in the $^{31}P$ NMR spectrum. For solubility reasons the reaction was studied in dichloromethane, giving one peak from **2** and one from what was identified as $[Pt_2I_4(PPh_3)_2]$ (all chemical shifts and coupling constants are given in Table 1). Addition of 2 equivalents of $NBu_4I$ caused the latter peak to disappear totally. Obviously there is an equilibrium in solution between the monomeric and bridged species. The initial UV/VIS spectrum of **2** in MeCN changes substantially upon addition of 10 equivalents of iodide; further addition causes only minor changes. This spectrophotometric change can most probably be ascribed to the same equilibrium as in dichloromethane, since the $^{31}P$ NMR spectrum of **2** in MeCN (not fully dissolved) only contains a peak from the monomeric species.

### Reaction with amines

Reaction (3) (E = P or Sb) was studied in MeCN using pyridine

$$[PtI_3(EPh_3)]^- + am \rightleftharpoons [PtI_2(EPh_3)(am)] + I^- \quad (3)$$

(py), 2- (2-mpy) and 4-methylpyridine (4-mpy) as incoming ligands. Less basic substituted pyridines (such as 3,5-dichloropyridine) caused no reaction to take place. Time-resolved spectra of the reactions of complexes **1** and **2** with pyridine are shown in Fig. 3. The products, compounds **3** and **4**, were prepared and characterised separately and their UV/VIS and $^{31}P$ NMR spectra were identical to those of the reaction products formed *in situ*. The compounds 2- and 4-mpy yielded products with spectroscopic properties very similar to those of **3** and **4** with one exception. The reaction of **2** with 2-mpy gives rise to two products as seen from $^{31}P$ NMR spectroscopy, and therefore this reaction was excluded from the kinetic study.

**Table 3** Details of the crystallographic data collection and refinement for complexes **1** and **2***

| | **1** | **2** |
|---|---|---|
| Chemical formula | $C_{34}H_{51}I_3NPtSb$ | $C_{34}H_{51}I_3NPPt$ |
| $M$ | 1171.3 | 1080.56 |
| $a$/Å | 9.668(2) | 9.724(1) |
| $b$/Å | 18.566(6) | 18.284(2) |
| $c$/Å | 22.045(9) | 21.614(2) |
| β/° | 98.42(3) | 98.487(8) |
| $U$/Å$^3$ | 3914(2) | 3800.8(6) |
| $F$(000) | 2200 | 2056 |
| $D_c$/g cm$^{-3}$ | 1.987 | 1.888 |
| μ/cm$^{-1}$ | 66.33 | 61.79 |
| Crystal size/mm | 0.25 × 0.12 × 0.10 | 0.15 × 0.10 × 0.10 |
| No. measured reflections | 8391 | 8175 |
| No. independent reflections | 8184 | 7968 |
| $h,k,l$ Ranges | −11 to 12, 0–23, −27 to 0 | −12 to 11, 0–22, 0–26 |
| Intensity variation in standard reflections (%) | −7.6 | −4.3 |
| $T_{min}$, $T_{max}$ | 0.608, 1 | 0.837, 0.998 |
| No. reflections used in refinement | 3466 | 2560 |
| σ cut-off | 2.5 | 2.0 |
| No. parameters | 361 | 361 |
| $R$ | 0.066 | 0.074 |
| $R'$ | 0.060 | 0.067 |
| $S$ | 2.04 | 1.84 |
| $\Delta\rho_{max}$/e Å$^{-3}$ | 1.97 | 2.23 |
| $(\Delta/\sigma)_{max}$ | 0.005 | 0.035 |

* Details in common: red prism; monoclinic; space group $P2_1/n$; $Z = 4$; $\theta_{max}$ 26.3°; $R = \Sigma(||F_o| - |F_c||)/\Sigma|F_c|$; $R' = [\Sigma w(|F_o| - |F_c|)^2/\Sigma|F_c|^2]^{\frac{1}{2}}$ with $w = 1/\sigma^2(F)$.

**Table 4** Selected crystallographic distances (Å) and angles (°) with estimated standard deviations in parentheses for complexes **1** and **2**

| | **1** (E = Sb) | **2** (E = P) |
|---|---|---|
| Pt–I(1) | 2.596(2) | 2.585(2) |
| Pt–I(2) | 2.637(2) | 2.662(3) |
| Pt–I(3) | 2.596(2) | 2.594(3) |
| Pt–E | 2.507(2) | 2.225(9) |
| E–C(1) | 2.16(2) | 1.86(3) |
| E–C(7) | 2.11(3) | 1.78(3) |
| E–C(13) | 2.11(3) | 1.82(3) |
| I(1)–Pt–E | 85.83(7) | 88.3(2) |
| I(1)–Pt–I(2) | 90.18(7) | 87.13(10) |
| I(2)–Pt–I(3) | 91.76(7) | 89.66(9) |
| I(3)–Pt–E | 92.71(7) | 95.5(2) |
| C(1)–E–C(7) | 98.0(9) | 99(1) |
| C(1)–E–C(13) | 97.5(9) | 100(1) |
| C(7)–E–C(13) | 103(1) | 104(1) |

Reaction (3) with complex **1** as a substrate is an equilibrium reaction. To determine the equilibrium constants given in Table 5, equation (4) was fitted to equilibrium absorbances at

$$A = \frac{A_0[I^-] + \varepsilon_b K_{eq}[am][Pt]_{tot}}{[I^-] + K_{eq}[am]} \quad (4)$$

different $[I^-]$ and [am]; $A_0$ denotes the absorbance before reaction takes place and the adjustable parameters are $\varepsilon_b$ (the molar absorption coefficient of the product at the pathlength used) and $K_{eq}$. For am = py, $K_{eq}$ was also determined at different temperatures and equation (5) was fitted to these data, giving the

$$\ln(K_{eq}) = \frac{\Delta S^\circ}{R} - \frac{\Delta H^\circ}{R}\frac{1}{T} \quad (5)$$

following thermodynamic parameters: $\Delta H^\circ = -22.2 \pm 1.4$ kJ mol$^{-1}$ and $\Delta S^\circ = -67 \pm 5$ J K$^{-1}$ mol$^{-1}$.

To avoid solvolysis of complex **1** during the kinetic experiments high iodide concentrations ($[I^-]/[Pt] > 70$) were used. In spite of this plots of $k_{obs}$ *vs.* [am] were non-linear in some cases, indicating the involvement of some steady-state intermediate, most probably the solvento species, **5**. The rate expression (6),

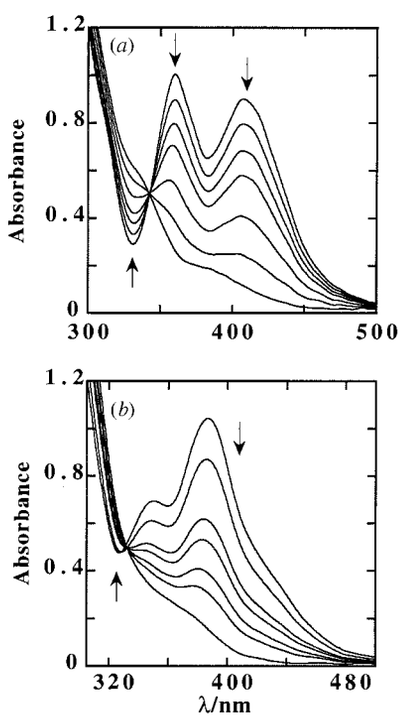


**Fig. 3** Time-resolved spectra for reaction (3) with pyridine as nucleophile at 298.2 K: (*a*) $[PtI_3(SbPh_3)^-] = 0.24 \times 10^{-3}$, $[py] = 30.9 \times 10^{-3}$, $[I^-] = 4.0 \times 10^{-3}$ mol dm$^{-3}$; scans obtained at 1.2, 6.2, 12.5, 18.8, 31.2, 50.0 and 200 ms; (*b*) $[PtI_3(PPh_3)^-] = 0.26 \times 10^{-3}$, $[py] = 38.6 \times 10^{-3}$, $[I^-] = 7.8 \times 10^{-3}$ mol dm$^{-3}$; scans obtained at 0.050, 0.62, 1.87, 2.50, 3.75, 5.0 and 20.0 s

$$k_{obs} = k_{12}([py] + K_{eq}^{-1}[I^-]) + \frac{K_{eq}k_{23}[py] + k_{23}[I^-]}{[I^-] + (k_{32}/k_{31})[py]} \quad (6)$$

with rate constants defined as in Scheme 1, was fitted to the data of $k_{obs}$ *vs.* [py] at different $[I^-]$. This was performed simultaneously for all data in a non-linear least-squares fashion using the program MATLAB.[22] By use of equation (7) the rate

$$K_{eq} = \frac{k_{12}}{k_{21}} = \frac{k_{13}k_{32}}{k_{23}k_{31}} \quad (7)$$

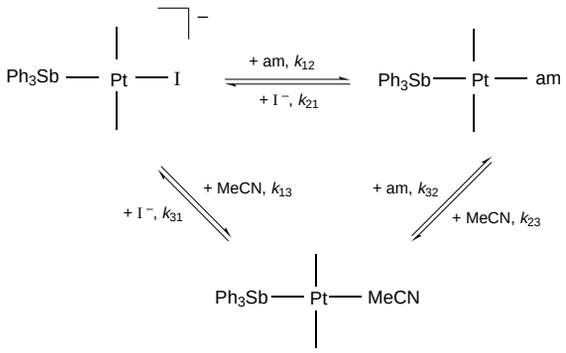


**Scheme 1**

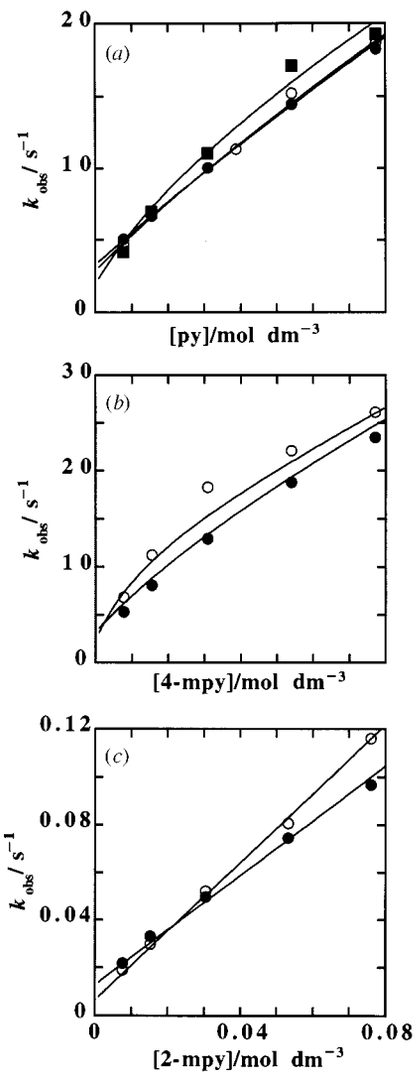


**Fig. 4** Observed pseudo-first-order rate constants for reaction (3) with complex **1** as substrate as a function of amine concentration at different iodide concentrations at 298.2 K: (*a*) am = py, $[I^-] = 10.0 \times 10^{-3}$ (■), $25.2 \times 10^{-3}$ (○) and $31.5 \times 10^{-3}$ mol $dm^{-3}$ (●); (*b*) am = 4-mpy, $[I^-] = 15.7 \times 10^{-3}$ (○) and $49.9 \times 10^{-3}$ mol $dm^{-3}$ (●); (*c*) am = 2-mpy, $[I^-] = 20.0 \times 10^{-3}$ (○) and $49.9 \times 10^{-3}$ mol $dm^{-3}$ (●)

constant $k_{13}$, which is common to all nucleophiles, can be calculated and equation (6) rewritten to contain only two unknown parameters, equation (8). Equation (8) was fitted to

$$k_{obs} = k_{12}([am] + K_{eq}^{-1}[I^-]) + \frac{k_{13}(k_{32}/k_{31})[am] + (k_{13}k_{32}/K_{eq}k_{31})[I^-]}{[I^-] + (k_{32}/k_{31})[am]} \quad (8)$$

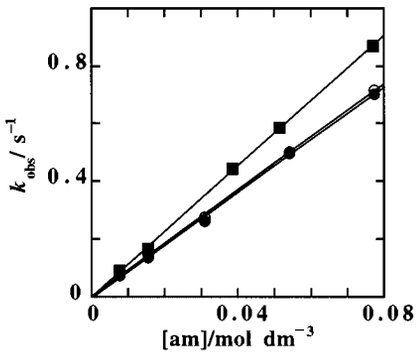


**Fig. 5** Observed pseudo-first-order rate constants for reaction (3) with complex **2** as substrate as a function of amine concentration at 298.2 K: (●) am = py, $[I^-] = 7.8 \times 10^{-3}$ mol $dm^{-3}$; (○) am = py, $[I^-] = 4.2 \times 10^{-3}$ mol $dm^{-3}$; (■) am = 4-mpy, $[I^-] = 5.0 \times 10^{-3}$ mol $dm^{-3}$

the experimental data for the incoming nucleophiles 2- and 4-mpy. Plots of all data with corresponding fits are shown in Fig. 4. Rate constants are given in Table 5. For am = py data were also collected at different temperatures. Equation (6) contains too many unknowns to make a fit feasible at a single iodide concentration. However, it can be assumed that the ratio between $k_{32}$ and $k_{31}$ is approximately independent of temperature, since these two rate constants refer to reactions of the same complex. Thus, using values of $K_{eq}$ calculated from equation (5) and the value of $k_{32}/k_{31}$ obtained at 25 °C, equation (6) was fitted to data for $k_{obs}$ *vs.* [py] at different temperatures giving values of $k_{12}$ and $k_{23}$. The rate constant $k_{21}$ was calculated from equation (7) and the activation parameters, given in Table 6, were derived for all three rate constants using the Eyring equation.

Reaction (3) with complex **2** as a substrate is not reversible. In Fig. 5 $k_{obs}$ is plotted *vs.* [am]. The usual two-term rate equation (9) was fitted to the data. Activation parameters were obtained

$$k_{obs} = k_{13} + k_{12}[am] \quad (9)$$

by fitting the Eyring equation to $k_{13}$ and $k_{12}$ (am = py) at different temperatures. From the plots in Fig. 5 $k_{13}$ can be taken as zero, but its smooth increase with temperature precludes such an interpretation. Values of rate constants are given in Table 5 and activation parameters in Table 6.

## Discussion

### Rate laws and mechanisms

The rate equation (9) for reaction (3) with complex **2** as substrate can be interpreted in terms of the usual two-term mechanism involving one direct attack by the nucleophile at the metal centre and one parallel attack by solvent. The intercept is very small in comparison to the nucleophile-dependent contribution, but its continuous increase with temperature is significant. For am = 4-mpy it is too small to be detected, which would speak in favour of an alternative interpretation, the intercept being a contribution from a reverse reaction. Such an interpretation is not compatible with the fact that the value of the intercept (am = py) is independent of $[I^-]$. Therefore, $k_{13}$ can be attributed to a solvent path.

For complex **1** the situation is more complicated; the reaction is reversible and there is a competition for the solvento complex. The more elaborate rate expression (6) can be rationalised in terms of the mechanism in Scheme 1 if the steady-state approximation is used for the solvento complex, **5**. Steady-state conditions are fulfilled for the high $[I^-]$ and [am] used in the kinetic runs. The fact that Fig. 3(*a*) shows a well defined isosbestic point further validates this approximation.

Equation (6) was fitted simultaneously at three different

**Table 5** Rate and equilibrium constants for reaction (3) at 25 °C in acetonitrile solvent

| | **1** | | | **2** | |
|---|---|---|---|---|---|
| | py | 2-mpy | 4-mpy | py | 4-mpy |
| $k_{12}$/dm$^3$ mol$^{-1}$ s$^{-1}$ | 145 ± 10 | 0.95 ± 0.02 | 197 ± 13 | 9.2 ± 0.2 | 11.3 ± 0.2 |
| $k_{21}$/dm$^3$ mol$^{-1}$ s$^{-1}$ | 61 ± 7 | 0.21 ± 0.01 | 27 ± 5 | | |
| $k_{32}/k_{31}$ | 0.27 ± 0.05 | (8.2 ± 0.6) × 10$^{-4}$ | 1.1 ± 0.3 | | |
| $k_{13}$/s$^{-1}$ | 12 ± 2 | | | 0.01 ± 0.003 | |
| $k_{23}$/s$^{-1}$ | 1.3 ± 0.3 | (2.2 ± 0.4) × 10$^{-3}$ | 1.8 ± 0.6 | | |
| $K_{eq}$ | 2.4 ± 0.2 | 4.5 ± 0.1 | 7.2 ± 1.2 | | |

**Table 6** Activation parameters for reaction (3) with pyridine as nucleophile

| Substrate | Rate constant | $\Delta H^{\ddagger}$/kJ mol$^{-1}$ | $\Delta S^{\ddagger}$/J K$^{-1}$ mol$^{-1}$ |
|---|---|---|---|
| **1** | $k_{12}$ | 11.6 ± 1.0 | −165 ± 4 |
| | $k_{21}$ | 33.7 ± 1.1 | −98 ± 4 |
| | $k_{23}$ | 32 ± 6 | −135 ± 17 |
| **2** | $k_{12}$ | 34.0 ± 0.4 | −112.6 ± 1.2 |
| | $k_{13}$ | 59.8 ± 3.6 | −82 ± 13 |

iodide concentrations for am = py, but still the values of $k_{23}$ and $k_{32}/k_{31}$ have large errors. The fits where $k_{13}$ was held constant [equation (8)] give more accurate values, but for am = 4-mpy the large error in $K_{eq}$ is propagated to some of the rate constants. In total, this means that some of the rate constants derived have relatively large errors.

The activation parameters are typical of associatively activated processes; all the entropies are largely negative and the enthalpies are low, in particular in the case of the stibine complex **1**. In fact the activation parameters for **1** (the $k_{12}$ path) are so extreme that it seems as if very little bond breaking has occurred in the transition state. The strongly associative behaviour also manifests itself in the large decrease of the rate of substitution in **1** on introducing an *o*-methyl group on the pyridine nucleophile (*cf.* rate constants $k_{12}$ in Table 5).

### Reactivity and *trans* effect

The *trans* effect is a well established concept in platinum(II) chemistry and a lot of ligands have been investigated with respect to this property. It is generally subdivided into a σ and a π contribution, the former chiefly affecting the ground state and the latter the transition state.[23,24] The σ-donating ability of donor atoms is known to decrease down the pnictogen group and stibines are also believed to be slightly weaker π acceptors than are phosphines.[2]

Having determined the mechanism of the reaction for both substrates it is now possible to include triphenylstibine in the *trans*-effect series, in which it clearly will end up before triphenylphosphine. This is in keeping with a previous report.[3] A qualitative *trans*-effect series including ligands that have been investigated in the context of similar systems as the one presented here would then be as follows:[13,25] $C_2H_4 > SbPh_3 > CO > P(OMe)_3 > PPh_3 > AsEt_3$. This series needs some comments. The position of the three ligands to the right is straightforward and taken directly from the literature.[13] The order of the other three calls for some more elaborate considerations. The reactivity ratio between $[PtI_3(PPh_3)]^-$ **2** and $[PtCl_3(PPh_3)]^-$ is about 2–3 : 1 depending on the nucleophile.[13] To compare $[PtI_3(SbPh_3)]^-$ **1** with other complexes with chloride as leaving group and methanol as solvent this factor has to be taken into account, and thus it seems as if triphenylstibine has a higher *trans* effect than that of $P(OMe)_3$, for in $[PtCl_3\{P(OMe)_3\}]^-$ in methanol chloride is substituted by pyridine with a rate constant of 190 dm$^3$ mol$^{-1}$ s$^{-1}$. To order the three first ligands in the *trans* series the reverse of reaction (3) has to be considered. A similar reaction, (10), has been investigated,[25]

$$[PtCl_2(py)L] + Cl^- \longrightarrow [PtCl_3L]^- + py \qquad (10)$$

giving rate constants of 20 300 ($C_2H_4$) and 2.9 dm$^3$ mol$^{-1}$ s$^{-1}$ (CO) as compared to the present value of $k_{21}$ = 61 dm$^3$ mol$^{-1}$ s$^{-1}$ for the stibine complex.

Once the *trans* effect of the stibine ligand has been established the question arises as how to rationalise it. As mentioned, high *trans* effects are normally explained in two ways. First, strong σ donation from a ligand, giving rise to a high ground-state *trans* influence, increases the rate of substitution. Secondly, charge delocalisation in the transition state helps to stabilise it and thus to increase the rate. Strong π acceptors typically give this kind of stabilisation, and thus have a high *trans* effect. To distinguish between these effects nucleophilic discrimination has been used as a criterion, usually expressed as the ratio between the rate constants for the direct and solvolytic pathways.[13] In acetonitrile, however, the solvent has been shown to give a very small contribution even for substitution *trans* to very strong σ donors (*e.g.* silyls).[9] This fact in combination with the relatively low accuracy of the $k_{13}$ values in the present study makes the ratio $k_{12}/k_{13}$ not very informative. The values of $k_{12}$ for 4-mpy and py could also be compared but it is known that the amine basicity plays a minor role in determining its nucleophilicity.[10,26,27] The calculated ratios are accordingly small and similar for **1** (1.4 : 1) and **2** (1.2 : 1), and it is difficult to draw any conclusions based on these values.

In view of these non-conclusive comparisons it is instead proposed that the *trans* influence and *trans* effect of the ligands be compared, the *trans* influence being used as a measure of the σ component. From spectroscopic data a decrease of the *trans* influence from $PPh_3$ to $SbPh_3$ has been inferred.[6] So far, no conclusive crystallographic data have been presented, but the clearcut difference in the Pt–I distances *trans* to the pnictogen E in **1** [2.637(2)] and **2** [2.662(3) Å] found here is consistent with the spectroscopic results and it can be definitely concluded that $SbPh_3$ has a smaller *trans* influence and hence acts as a weaker σ donor than does $PPh_3$. The only reasonable explanation for the high *trans* effect of the stibine is therefore that it has a better ability to accept charge and thereby stabilise the five-co-ordinate transition state. This is in keeping with the well known fact that stibines stabilise five-co-ordination also in the ground state.[28,29] From the present results it is thus reasonable to conclude that this property is due to a better π acceptance, both in the ground and transition states, rather than to a weaker σ donation as proposed earlier.[1]

To measure σ and π contributions to M–P bonds of $PA_3$ complexes in the ground state the P–A distances and A–P–A angles have been successfully used.[30] This is rationalised by the fact that the π-acceptor function on the phosphorus is a mixture of P–A σ* and phosphorus 3d orbitals.[31,32] Increasing π acceptance therefore leads to longer P–A distances and smaller A–P–A angles, whereas the opposite is true for increasing σ donation. As shown by Orpen and co-workers[30] these two effects almost cancel for Pt–$PPh_3$ complexes and the average distances and angles in the complexes are approximately the same as in free $PPh_3$. Data for $SbPh_3$ are obviously more scarce but an examination of the three crystal structures of Pt–$SbPh_3$

complexes available[4] (including the present one of compound **1**) reveals an average Sb–C distance and C–Sb–C angle of 2.120(15) Å and 102.0(3.7)°, respectively (for 21 distances and angles). The values for free triphenylstibine are 2.155(9) Å and 96.3(1.2)°, respectively,[33] and it can be concluded that using a 95% confidence level the average Sb–C distance in the platinum complexes is significantly shorter than the average distance in free $SbPh_3$, whereas the difference in C–Sb–C angles is not statistically significant, although there is a trend towards larger angles in the complexes. In analogy with the phosphine complexes this could be taken as evidence for a higher σ/π ratio in the Pt–Sb bond, but this is not in accordance with the above conclusion about the π-accepting ability of stibines. Instead we propose that these structural observations be explained by assuming that the π* orbital on antimony has a much smaller contribution from the Sb–C σ* orbital and is predominantly of 5d character. This also gives a reasonable explanation for the observed *trans* effects of pnictogen ligands. As noted arsines have a lower *trans* effect than phosphines, which is explained by their lower *trans* influence (and possibly a lower π-accepting ability). On going from arsines to stibines the *trans* effect increases dramatically. Using the above assumption on the antimony π* orbitals, this can be nicely explained by the very good overlap that is expected between the filled platinum 5d and empty antimony 5d orbitals.

## Acknowledgements

We thank Dr. Åke Oskarsson for valuable discussions of this work and Mr. Per-Henrik Myrefelt for help with the computer program MATLAB. Financial support from the Swedish Natural Science Research Council is gratefully acknowledged.

## References

1 N. R. Champness and W. Levason, *Coord. Chem. Rev.*, 1994, **133**, 115.
2 W. Levason and C. A. McAuliffe, *Acc. Chem. Res.*, 1978, **11**, 363.
3 T. P. Cheeseman, A. L. Odell and H. A. Raethel, *Chem. Commun.*, 1968, 1496.
4 O. F. Wendt, A. Scodinu and L. I. Elding, *Inorg. Chim. Acta*, 1997, in the press.
5 T. G. Appleton, H. C. Clark and L. E. Manzer, *Coord. Chem. Rev.*, 1973, **10**, 335.
6 T. G. Appleton and M. A. Bennett, *Inorg. Chem.*, 1978, **17**, 738.
7 O. F. Wendt, Å. Oskarsson, J. G. Leipoldt and L. I. Elding, *Inorg. Chem.*, 1997, **36**, 4514.
8 O. F. Wendt, Ph.D. Thesis, Lund University, 1997.
9 O. F. Wendt and L. I. Elding, *Inorg. Chem.*, 1997, **36**, in the press.
10 R. Romeo and M. L. Tobe, *Inorg. Chem.*, 1974, **13**, 1991.
11 B. P. Kennedy, R. Gosling and M. L. Tobe, *Inorg. Chem.*, 1977, **16**, 1744.
12 R. Gosling and M. L. Tobe, *Inorg. Chim. Acta*, 1980, **42**, 223.
13 R. Gosling and M. L. Tobe, *Inorg. Chem.*, 1983, **22**, 1235.
14 M. L. Tobe, A. T. Treadgold and L. Cattalini, *J. Chem. Soc.*, *Dalton Trans.*, 1988, 2347.
15 P. L. Goggin, R. J. Goodfellow and F. J. S. Reed, *J. Chem. Soc.*, *Dalton Trans.*, 1972, 1298.
16 P. L. Goggin, *J. Chem. Soc.*, *Dalton Trans.*, 1974, 1483.
17 W. Baratta and P. S. Pregosin, *Inorg. Chim. Acta*, 1993, **209**, 85.
18 TEXSAN, Structure Analysis Software, Molecular Structure Corporation, The Woodlands, TX, 1985.
19 Bio Sequential SX-17MV Stopped flow ASVD Spectrofluorimeter, software manual, Applied Photophysics, Leatherhead, 1994.
20 D. A. Duddell, P. L. Goggin, R. J. Goodfellow, M. G. Norton and J. G. Smith, *J. Chem. Soc. A*, 1970, 545.
21 C. K. Johnson, ORTEP, Report ORNL-5138, Oak Ridge National Laboratory, Oak Ridge, TN, 1976.
22 MATLAB 4.2, The Math Works, Inc., Natick, MA, 1995.
23 F. Basolo, J. Chatt, H. B. Gray, R. G. Pearson and B. L. Shaw, *J. Chem. Soc.*, 1961, 2207.
24 C. H. Langford and H. B. Gray, *Ligand Substitution Processes*, W. A. Benjamin, New York, 1965.
25 L. Canovese, M. L. Tobe and L. Cattalini, *J. Chem. Soc.*, *Dalton Trans.*, 1985, 27.
26 L. Cattalini, A. Orio and A. Doni, *Inorg. Chem.*, 1966, **5**, 1517.
27 L. Canovese, L. Cattalini, G. Marangoni, G. Michelon and M. L. Tobe, *Inorg. Chem.*, 1981, **20**, 4166.
28 A. D. Westland, *J. Chem. Soc.*, 1965, 3060.
29 C. A. McAuliffe, I. E. Niven and R. V. Parish, *Inorg. Chim. Acta*, 1975, **15**, 67.
30 B. J. Dunne, R. B. Morris and A. G. Orpen, *J. Chem. Soc.*, *Dalton Trans.*, 1991, 653.
31 D. S. Marynick, *J. Am. Chem. Soc.*, 1984, **106**, 4064.
32 A. G. Orpen and N. G. Connelly, *Organometallics*, 1990, **9**, 1206.
33 E. A. Adams, J. W. Kolis and W. T. Pennington, *Acta Crystallogr.*, *Sect. C*, 1990, **46**, 917.

*Received* 11*th September* 1997; *Paper* 7/06617A